Diego FONSÊCA[1], Andres SALAZAR[1], Tomaz GONÇALVES[1], Elmer VILLARREAL[2]

Federal University of Rio Grande do Norte (1), Federal University of the Semi-Arid (2), Brazil

doi:10.15199/48.2019.10.04

Electrical modelling of an electrical submersible pump system three-phase power cable used in power line communication

Abstract. *In this paper, an analysis of electrical parameters of a 2036 m ESP three-phase power cable and round profile has been carried out. This analysis will provide subsidies to electrically model the channel through which the data will be transmitted from downhole to the surface. A printed circuit board was developed through the correct grouping of passive electronic components to represent the same impedance and phase behavior of the measured ESP power cable for a frequency range from 20 Hz to 200 kHz.*

Streszczenie. *W artykule nalizowany jest system komunikacji w zanurzeniowej pompie zasilanej napieciem trójfazowy za pośrednictwem kabla. Ten sam kabel jest też wykorzystywany do przesyłania sygnałów z czujników.* ***Model elektryczny pompy zanurzeniowej w której kabel zasilający wykorzystywany jest do komunikacji.***

Keywords: electrical submersible pump, three-phase power cable, artificial lift, impedance analysis.
Słowa kluczowe: pompa zaniurzenmiowa, kabel zasilahjący, przesyłanie danych.

Introduction

Electrical submersible pumps (ESPs) are commonly used artificial lift method in deep wells in oil industry. ESPs are typically installed in oil wells ranging from a few hundred to a few thousand feet deep [1].

In the ESP artificial lift method the electric energy is transmitted to the bottom of the well through a cable, where it is transformed into mechanical energy by a subsurface motor. This motor is connected to a centrifugal pump, which transmits the energy to the fluid in the form of pressure, lifting it to the surface. Fig. 1 shows the structure of a ESP well with its main components.

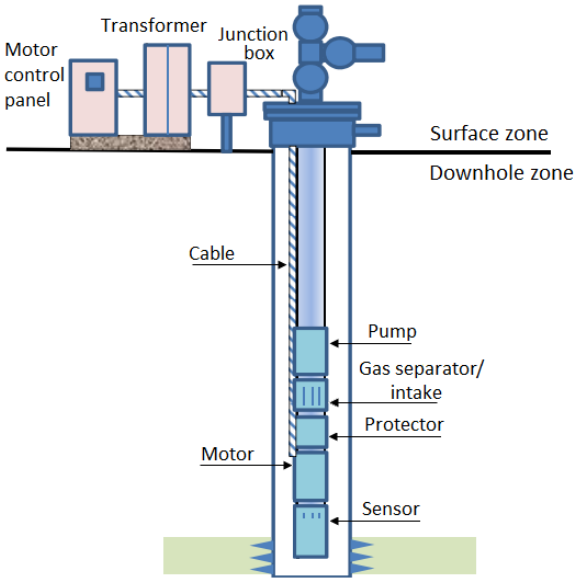

Fig.1. Typical Electrical Submersible Pump system and main components.

To assist in optimizing production, gathering equipment lifetime data gathering and to ensure optimal ESP performance, operators may install downhole sensors that continuously acquire real-time system measurements such as pump intake and discharge pressures and temperatures, vibration, current leakage rate [1, 2, 3] and contamination of insulating oil in motors [4, 5]

The downhole monitoring tools are used to transmit the read data to the surface. They are connected to the neutral of the electrical submersible motor at the bottom of the ESP string and send signals through the main power cable to the surface read out unit.

One comon downhole monitoring tool design used in the field is to utilize a modulated DC loop current over the three-phase power cables to transmit data between the downhole sensors and the surface monitoring electronics unit. The downhole tool is connected to the Y-point of the ESP motor and to the ground of the downhole system [5, 6].

In this dc communication scheme, the surface electronic device provides DC power to the downhole sensor circuitry over the main power cable with the ground serving as the return path. The main power cable and surface electronic device are separated through a DC choke [1, 3].

Downhole sensors, designed in the form of a current sink, retrieve the dc power from the neutral-point of the submersible motor and modulate the current signal. The surface electronic devices determine downhole conditions by detecting and measuring the modulated current signal [1, 3].

In this paper an electrical model is proposed that accurately reproduces the electrical impedance and phase behavior of a ESP cable 2,036 m long for a specific frequency range. The model will allow a more thorough analysis of the channel in order to obtain points of low impedance and, make it possible an increase in the transmission rates of the data to the surface.

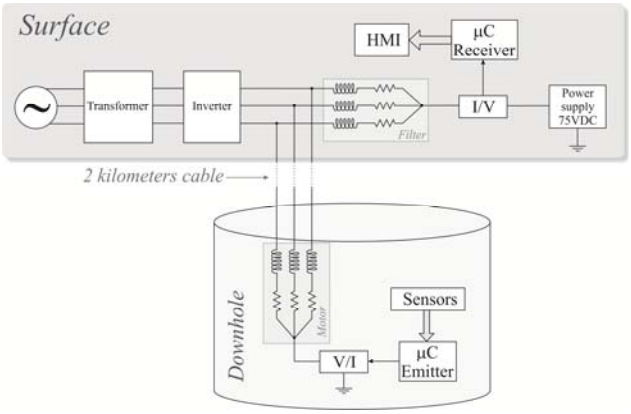

Fig.2. Overview of ESP communication modules.

ESP System Configuration With the Proposed Communication Channel and Electrical Modules

The collected data will be sent to the surface through a communication system as showed in Fig. 2. The downhole sensor, formed by the sensors, microcontroller emitter and voltage-current converter *(V/I)*, is connected to the neutral of the motor. At this point a DC (Direct Current) current signal is inserted by the downhole sensor, which will flow over the three phases of the electrical supply cable. On the surface, a three-phase Y connection inductive filter acts as an interface for withdrawing the DC current signal, as well as removing signals at the fundamental frequency. The current signal is available to the surface module formed by the current-voltage converter (*I/V*), the microcontroller receiver and the 75 V_{DC}, power supply, which is responsible for powering the electronics on the downhole sensor.

Impedance of three-phase ESP power cable

The data transmission rate on the ESP systems varies from 5 to 10 bits/s [7]. This data transfer rate is adopted due to the physical layer provided by the ESP system, which acts as a low-pass filter with a cutoff frequency of 10 Hz.

In this sense, a more accurate analysis of the channel, which is the three-phase cable itself, is required. However, given the difficulty of access to ESP equipment as a cable and motor, the proposal is to design an electronic circuit that reproduce the same electrical behavior (impedance and phase as a function of frequency) of a ESP cable. In this paper, was focused only in the modeling of the power cable. The Impedance measurements was carried out for a low votlage power cable. The cable length was 2036 meters, three-phase 4 AWG and flat profile. The cable was measured in the following signal couplings: L_1 e L_2. The input impedance was measured when the L_1 and L_2 ends was short-circuited and when they were open, the signal being injected into L_1 and returned by L_2. The measured frequency band was 20 Hz – 10 MHz and a linear frequency sweep was applied. The impedance analyser Keysight E4990A stored 500 data points (frequency, absolute value and phase) for each measurement.

The impedance measurement with signal coupling $L_1 - L_2$ and cable end short-circuited is illustrated in Fig. 3.

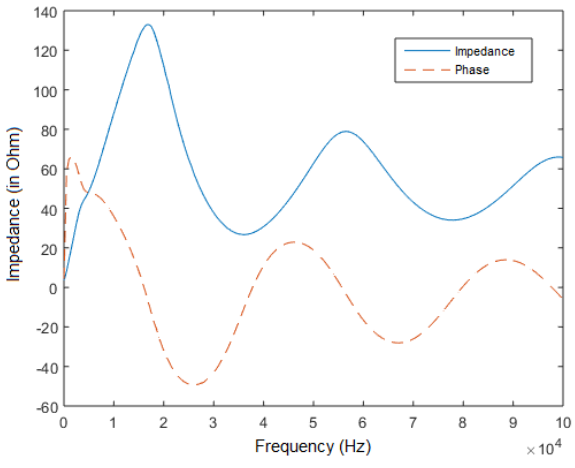

Fig.3. Input impedance (continuous line) and phase (dashed line) as a function of frequency for the low voltage power cable with signal coupling $L_1 - L_2$ and cable end short-circuited.

Fig. 3 shows the repetition of peaks and slopes in the impedance curve. At the impedance peak, the cable behaves as a parallel resonant circuit and at the point of slope presents the characteristic of a series resonant circuit.

In case of no losses in the cable the input impedance of the circuit would be infinite when it was in parallel resonant. The input resistance, in this case, should have a very high value (infinity) for the current to flow into the capacitive and inductive components without loss of energy by resistive components, resulting in the desired resonance. The same goes for the series resonant circuit. Thus, to have a perfect resonance between the inductors and capacitors, the input impedance value should be zero for the current to flow to the resonant components without losing power. Therefore, if the load and discharge of the capacitor occur without losses, the cycle would occur for infinite time. As a consequence a sinusoidal signal would be generated and it frequency would depend on the values of the capacitor and the inductor. In practice, however, the inductor leads and circuit resistors represent a resistance that absorbs energy. Thus, the oscillation that occurs is cushioned until it disappears.

Influence of parasitic elements

All real components have their frequency-dependent values due to the existence of parasitic elements. However, not all parasitic elements affect measurements, but some more prominent determine the frequency response of the component. The prominent parasitic elements will be dominant when the impedance value of the primary element is no longer the same [7]. According to [8], in relation to capacitors, the inductive parasite series (L_S) is the main cause of the frequency response. At low frequencies, the impedance phase angle (q) is about *-90°*, thus, the reactance is capacitive.

The capacitor frequency response has a minimum impedance point at a self-resonance frequency (SRF), which is determined from the capacitance and parasitic inductance of a series equivalent circuit model for the capacitor [7]. At the self-resonance frequency, the capacitive and inductive reactance values are the same, according to equation 1.

$$\frac{1}{\omega \times C} = \omega \times L_S \tag{1}$$

where: ω – Angular frequency, C – capacitance, L – series parasitic inductance.

As a result, the phase angle is $0°$ and the device is resistive. After the resonant frequency, the phase angle changes to a positive value around $+90°$ and, therefore, the reactance becomes inductive due to the parasitic inductance being predominant.

Capacitors behave as inductive devices at frequencies above the SRF and as a result can not be used as capacitors at these particular frequencies [7]. Likewise, about the inductors, the parasitic capacitance causes a typical frequency response. Due to the parasitic capacitance (C_P), the inductor has a maximum impedance point at the SRF, where

$$\omega \times L = \frac{1}{\omega \times C_P} \tag{2}$$

where: ω – Angular frequency, C – parallel parasitic capacitance, L –inductance.

In the low frequency region (below the SRF), the reactance is inductive. After the self-resonance frequency, the parasitic capacitance becomes dominant and the reactance becomes capacitive. The SRF determines the maximum usable frequency of capacitors and inductors.

At frequencies above the SRF, a negative inductance value is displayed because the measured inductance value (L_m) is calculated from a capacitive reactance vector, which is te opposit of the inductive vector. The same happens for the measured capacitance values (C_m) when they pick frequencies above the SRF, since these are now calculated from an inductive reactance vector. Therefore, analyzing the obtained data, can be see that at resonance frequency, the values of inductances are negative, then it means that the parasite capacitance predominates in relation to the inductance.

As it can be seen in Fig. 3 the phase tends to become negative as it approaches the respective resonant frequencies. It is known that the phase is zero in the resonant frequency, however soon after this frequency, the value tends to be negative, showing again that the parasite capacitance predominates. In addition, it is noted that after the frequency starts to approach the resonance frequency of a series circuit (in this case, 36 kHz), the phase value starts to increase again and becomes positive, indicating that the inductance is predominating. And so the cycle repeats itself by going through all the resonance points. The inductor together with the parasitic capacitor in parallel, form the peaks of the impedance curves and the capacitor together as series parasitic inductor, form the slopes of the impedance curves.

Electrical model of ESP three-phase power cable

The methodology used to find the capacitance, inductance and resistance values was to fix an inductance value that represents the same inductance value of the ESP cable, and then find the value of the parasite capacitance.

However, the L_S data obtained from the impedance analyzer indicated that the inductance varies greatly according to frequency. This behavior is due to the fact that: the higher the frequency and the closer to the (parallel) resonance frequency, the lower the influence of the inductor and the greater the influence of the parasitic components (in this case, C_P). The inductor has an initial fixed value, however when the frequency is increasing its inductance becomes smaller Therefore, to find a fixed inductance value representing the first impedance curve, the mean of all L_S values until the exact moment before the first resonance (16.52 kHz), since after this ferquency L_S becomes negative. The same method was used for the second impedance curve and the mean of all L_S positive values at the exact moment before the second resonance (56.51 kHz) The inductance values calculated were 1 mH for the first resonance frequency and 0.44 μF. On the basis of these values it was possible to calculate the values (from Equation 3) of the parasitic capacitances associated to each inductance, referred to in the Table 1.

$$f_r = \frac{1}{\sqrt{L \times C} \times 2\pi} \quad (3)$$

where: f_r – resonant frequency, L – inductance, C – capacitance.

Table 1. Inductance and parasitic capacitance values for resonant frequencies

Resonant frequency (f_r)	Parasitic capacitance (C_P)	Inductance (L)
16.51 kHz	0.0930 μF	1 mH
56.52 kHz	0.1803 μF	0.44 μH

After obtaining the values of the components for each resonant frequency, the circuit representing the three-phase cable was implemented at first in a simulation software (see Fig. 4).

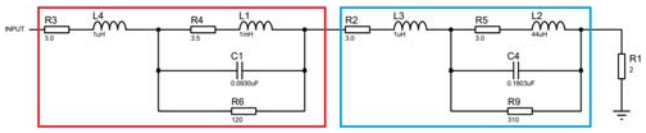

Fig.4. Electrical model of three-phase cable in simulation software.

The red and blue meshes represent, respectively, the electrical models for the resonance frequencies in the first and second curve in Fig. 3.

The 3 Ω resistances at the beginning of each meshe were placed to simulate the low resistive value presented by the evaluated ESP cable. The 1 μH inductance in series with the resistors represent parasitic inductances read from the data collected from the impedance analyzer. For low resistance values the series parasitic inductances arise as the frequency increases. If the resistance had a high value, a parasitic capacitance would appear in parallel with this resistance [8]

The parasitic resistances values in series with the inductance (3.5 Ω e 3.0 Ω), provided by the impedance analyzer, represent the minimum impedance and they are determined by the winding resistance (R_S). At the lower frequencies, the inductive reactance (ωL) decreases so that inductive winding resistance will be the inductance value [8].

The parasitic parallel resistances (R_P) with the inductance and capacitance (120 Ω e 310 Ω), provided by the impedance analyzer, represent the magnetic loss of the inductor core.

The resistance value connected to earth was chosen with a low value (2 Ω) simulates a shortcut to ground.

Once the data and graphs of the simulation software were obtained, a printed circuit was produced by combining resistors, inductors and capacitors of commercial values to reproduce the results of the simulation. As the components are manufactured with already defined values, it was necessary to group them in order to find the closest possible values of the previously calculated values as shown in Fig 5.

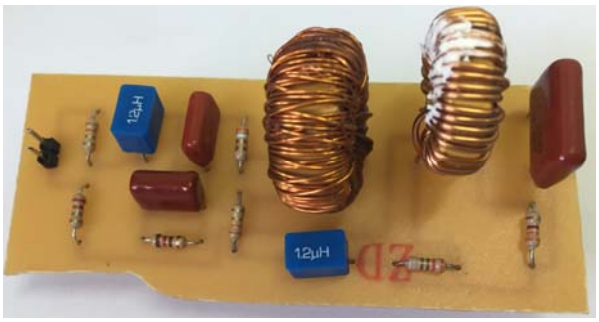

Fig.5. Printed circuit board (PCB) used for representing the electrical modelo f the ESP cable

The electronic components assembled on the PCB had commercial values closer to those found for the model were used. In the circuit of Fig. 6 present the value of each component.

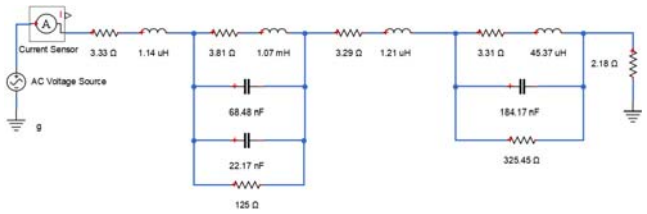

Fig.6. Schematic circuit with the real measured values of the components

Results

For an initial analysis of the proposed model, simulations were carried out in the same frequency range used to measure the actual cable parameters, from 20 Hz a 10 MHz. However, it was observed that from 200 kHz there was no other resonance frequency. This value was therefore used as the maximum frequency. Fig. 7 shows the result obtained.

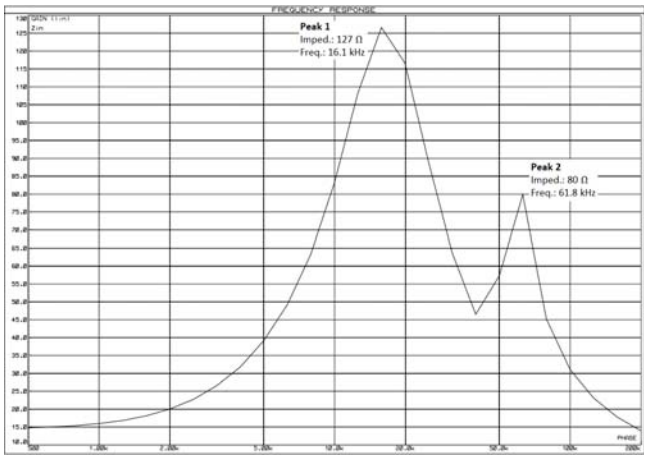

Fig.7. Impedance curve from the simulated circuit for a frequency of 20 Hz to 200 kHz.

A printed circuit board has been designed to reproduce the same impedance behavior of the ESP cable. Its implementation has been based on the data provided by the impedance analyzer and simulation results. Fig. 8 shows the behavior of the impedance obtained with the printed circuit board.

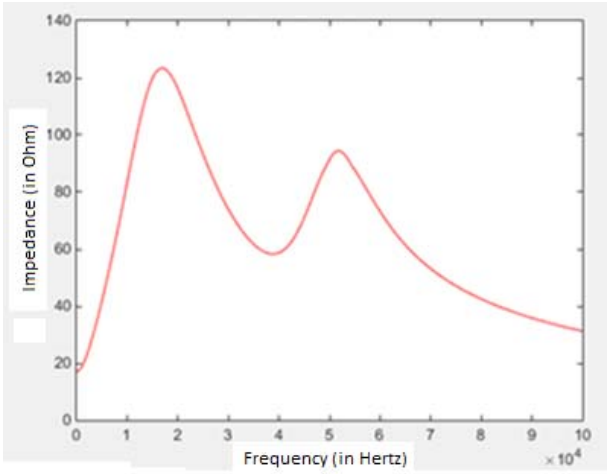

Fig.8. Impedance behavior measured on the printed circuit board at a frequency range from 20 Hz to 10 MHz.

Analyzing the characteristic impedance curve, it was verified that there is a similarity in the behavior of this parameter for the cable, the simulation and the proposed electric model.

Despite presenting similar impedance values, small deviations have been observed. These differences are due to the use of commercial components as well as the sensitivity of the resonance frequency to any difference in the inductance and capacitance values. At the first resonance peak the calculated real values (1.07 mH e 90.65 nF) were close to the calculated theoretical values (1 mH e 93 nF). However, as observed in Fig. 8, the values of the components responsible for the second peak curve (45.37 μH e 184.17 nF) would result in a resonance frequency around 54.8 kHz (according to Eq.01). So we can say that the second peak curve achieve the expected values.

Table 2 presents a comparison between the impedance vaues (Z) at the resonance frequencies (f_r) for the ESP cable, the simulation and the PCB. Table 3 shows the relative percent errors for the resonance frequency and inductance indicated in Table 2.

Table 2. Comparison between the resonance frequency and the impedance for the ESP cable, simulation and printed circuit board.

f_r cable [kHz]	Z cable [Ω]	f_r simul. [kHz]	Z simul. [Ω]	f_r circuit [kHz]	Z circuit [Ω]
16.51	133	16.1	126	17.02	123.5
56.52	79	61.8	80	52.01	92.77

Table 3. Relative percent errors for the resonance frequency and impedance referring to Table 2.

Error f_r simul. [%]	Error Z simul. [%]	Error f_r circuit. [%]	Error Z circuit [%]
2.48	5.26	3.09	7.14
9.34	1.26	7.97	17.43

According to Table 3 it is possible to observe that in some situations the errors have approached to and even passed the 10% mark. In the case of the simulation, the output should match the values found for the cable. This difference is due to the fact that the inductance and capacitance values are calculated from the average of the points collected up to a point before the resonance frequency, not precisely a single point.

The errors presented by the printed circuit are due to the inaccuracies of the electronic components used. In situations that did not have a component with the correct value, either an approximate value was used, or an association that provided the value close to the appropriate value.

Conclusions

It is possible to represent a three-phase cable for Electrical Submersible Pump through the appropriate association of inductors, capacitors and resistors.

The methods used to calculate the values of the passive components were correctly applied because the results obtained in both the simulation and the cable emulator circuit were acceptable.

For cables whose length is significant, it is more feasible to analyze electrical parameters through a current signal instead of voltage signal. Because, due to the cable size, the signal will have a voltage drop along it and the analysis will be faulty.

***Authors**: Eng. PhD. Diego A. M. Fonsêca, prof. PhD. Andres O. Salazar, Eng. Tomaz R. Gonçalves, Department of Computer Engineering and Automation, Federal University of Rio Grande do Norte, Natal/RN, Brazil, ZIP 59072-970, e-mail diegomoura@dca.ufrn.br, andres@dca.ufrn.br, tomazrochag@gmail.com; prof. PhD. Elmer R. L. Villarreal, Exact and Natural Sciences Center, Federal University of the Semi-Arid, Mossoró/RN, Brazil, ZIP 59625-900, e-mail elmerllanos@ufersa.edu.br*.

REFERENCES

[1] O. Ghoreishi, X. Liang and W. Xu, "Phase-to-Phase Communication Scheme for Downhole Monitoring Tool Design in Electrical Submersible Pump Systems", *IEEE Transactions on Industry Applications*, vol. 52, no. 3, pp. 2077-2087, 2016. Available: 10.1109/tia.2016.2527724

[2] Flatern, R., The Defining Series: ElectricalSubmersible Pumps (2015).

[3] F. Quintaes, A. O. Salazar, A. L. Maitelli, F. Fontes, M. A. A. Vieira, T. Eslley, "Magnetic sensor used to detect contamination of inulating oil in motors applied to electrical submersible pump*",IEEE Transactions on Magnetics*, vol. 47, no. 10, pp. 3756-3759, Oct. 2011. Available: 10.1109/TMAG.2011.2154359

[4] A. O. Salazar, D. A. M. Fonsêca, A. L. Martelli, F. Fontes and F. de Oliveira Quintaes, "Instrumentation to detect contamination of insulating oil in motors applied to electrical submersible pump", *2014 11th IEEE/IAS International Conference on Industry Applications, Juiz de Fora, 2014, pp. 1-7*.Available: 10.1109/INDUSCON.2014.7059440

[5] X. Liang, O. Ghoreishi and W. Xu, "Downhole Tool Design for Conditional Monitoring of Electrical Submersible Motors in Oil Field Facilities", *IEEE Transactions on Industry Applications*, vol. 53, no. 3, pp. 3164-3174, 2017. Available: 10.1109/tia.2016.2613984

[6] X. Liang, and W. Xu, "Downhole Tool Design for Conditional Monitoring of Electrical Submersible Motors in Oil Field Facilities", *IEEE/IAS 51st Industrial & Commercial Power Systems Technical Conference (I&CPS)*, 2015. Available: 10.1109/ICPS.2015.7266427

[7] D. Fonsêca, "Implementação de Sistema de Transmissão de Dados Através da Linha de Potência dos Poços com o Método de Elevação Bombeio Centrífugo Submerso", *master's thesis,* Federal University of Rio Grande do Norte, Aug 2018

[8] Keysight Technologies, *Impedance Measurement Handbook - A guide to measurement technology and techniques*, 6. ed. Santa Rosa, CA, 2016. Available in: <http://literature.cdn.keysight.com/litweb/pdf/5950-3000.pdf?id=1000075407:epsg:dow>. [Accessed 18 August 2017]